JVSTB Journal of Vacuum Science & Technology B

Lipid specific molecular ion emission as a function of the primary ion characteristics in TOF-SIMS

Kendra J. Adams, John Daniel DeBord, and Francisco Fernandez-Lima

Citation: Journal of Vacuum Science & Technology B **34**, 051804 (2016); doi: 10.1116/1.4961461
View online: http://dx.doi.org/10.1116/1.4961461
View Table of Contents: http://scitation.aip.org/content/avs/journal/jvstb/34/5?ver=pdfcov
Published by the AVS: Science & Technology of Materials, Interfaces, and Processing

Lipid specific molecular ion emission as a function of the primary ion characteristics in TOF-SIMS

Kendra J. Adams and John Daniel DeBord
Department of Chemistry and Biochemistry, Florida International University, Miami, Florida 33199

Francisco Fernandez-Lima[a)]
Department of Chemistry and Biochemistry, Florida International University, Miami, Florida 33199 and Biomolecular Science Institute, Florida International University, Miami, Florida 33199

(Received 12 May 2016; accepted 9 August 2016; published 24 August 2016)

In the present work, the emission characteristics of lipids as a function of the primary ion cluster size and energy were studied using time-of-flight secondary ion mass spectrometry (TOF-SIMS). Characteristic fragmentation patterns for common lipids are described, and changes in secondary ion (SI) yields using various primary ion beams are reported. In particular, emission characteristics were studied for pairs of small polyatomic and nanoparticle primary ion beams (e.g., Bi_3^+ versus Ar_{1000}^+ and Au_3^+ versus Au_{400}^{+4}) based on the secondary ion yield of characteristic fragment and intact molecular ions as a function of the lipid class. Detailed descriptions of the fragmentation patterns are shown for positive and negative mode TOF-SIMS. Results demonstrate that the lipid structure largely dictates the spectral presence of molecular and/or fragment ions in each ionization mode due to the localization of the charge carrier (head group or fatty acid chain). Our results suggest that the larger the energy per atom for small polyatomic projectiles (Bi_3^+ and Au_3^+), the larger the SI yield; in the case of nanoparticle projectiles, the SI increase with primary ion energy (200–500 keV range) for Au_{400}^{+4} and with the decrease of the energy per atom (10–40 eV/atom range) for $Ar_{n=500\text{-}2000}^+$ clusters. The secondary ion yield of the molecular ion of lipids from a single standard or from a mixture of lipids does not significantly change with the primary ion identity in the positive ion mode TOF-SIMS and slightly decreases in the negative ion mode TOF-SIMS.
 [http://dx.doi.org/10.1116/1.4961461]

I. INTRODUCTION

Secondary ion mass spectrometry (SIMS) is the gold standard for surface analysis of biological samples with submicron spatial resolution.[1–6] Over the years, the primary ion beam of choice has changed as new ion sources have been developed and capabilities by application (e.g., organic versus inorganic surfaces) have been documented.[7–9] For example, atomic and small polyatomic projectiles have shown distinct advantages for high spatial resolution, while larger clusters and nanoparticle projectiles have shown enhanced molecular ion emission.[7,8,10–12] In addition, for the analysis of biological surfaces, the reduced damaged cross section of some nanoparticle projectiles (e.g., C_{60}, argon, and water clusters) has triggered recent developments for tridimensional biological imaging and profiling.[7,13–17] For example, a continuous Ar_{1000}^+ beam provides a somewhat "softer" desorption process which reduces the internal energy imparted to desorbed molecules, resulting in significant improvements of molecular ion or pseudomolecular ion yields. These types of molecular ions tend to be more diagnostic for structural characterization and identification of the biological systems from which they are generated.[18] It has been reported that for an argon cluster beam, ideal ion yields are achieved when $E_{atom} \geq 10$ eV and ion yields will quickly decline as the E_{atom} decreases.[15] It was also observed that when water molecules are used as primary ion beams, the optimal energy was about 3 eV/atom, which leads authors to believe that further exploration into larger cluster projectiles is possible.[15] During the study of peptides using various primary ion energies of an argon cluster, it has been shown that larger peptide fragments were observed with lower energy beams as long as they were above 10 eV/atom; in addition, the fragment intensity tends to decrease with increasing mass at 20 or 40 eV/atom.[18]

Lipid profiling of biological samples is traditionally based on liquid extraction followed by liquid chromatography coupled to mass spectrometry (MS), with the collision induced dissociation spectra providing the necessary structural identification of the lipid class.[19–21] Alternatively, we have recently shown that lipid identification can be performed using direct surface probe analysis [matrix-assisted laser desorption/ionization (MALDI)], coupled to ultrahigh resolution mass spectrometry [Fourier transform ion cyclotron resonance mass spectrometry], followed by statistical analysis of variability and reproducibility across batches using internal standards.[22] Lipid assignment from MS data can be performed utilizing the LIPIDMAPS database, where lipids are divided into eight major classes: fatty acyls (FA), glycerolipids, glycerophospholipids, sphingolipids, sterol lipids (ST), prenol lipids, saccharolipids, and polyketides.[23–25] Analogous to MALDI probes, SIMS allows for *in situ* analysis of native biological surfaces, with higher spatial resolution. Due to the nature of molecular ion emission during SIMS analysis (not as soft as MALDI), fragmentation and intact molecular ion emission can be observed, with relative

[a)]Electronic mail: fernandf@fiu.edu

intensities varying with projectile size and energy. That is, the selection of the primary ion and energy determines the energy deposited per surface layer and the desorption volume, which corresponds to the observation of specific secondary ions (SIs).[26,27] For example, during the analysis of lipid components from a biological surface, analyte specific fragment ions (lipid head groups and fatty acid fragments) are mainly observed under monoatomic and small polyatomic bombardment (e.g., In, Ga, Cs, Au_3^+, Bi_3^+, sources)[28] while lipid molecular ions are increased under larger projectile bombardment (e.g., C_{60} and Au_{400}^{+4}). In a comparison of 40 keV C_{60}^+ to 40 keV Ar_{4000}^+ by Angerer and coworkers, it was observed that a majority of intact lipids from mouse brain were seen at higher secondary ion yields with the Ar_{4000}^+ primary ion, which is the primary ion beam that provided the larger cluster size but lower E_{atom}.[29] This study also analyzed the signal of the pseudomolecular ion of cholesterol $[M+H-H_2O]^+$ using the aforementioned primary ion species and observed that similar secondary ion yields were detected for both of the projectiles; however, using Ar_{4000}^+, a lower yield in the smaller lipid fragments was observed.[29]

In the present paper, we study the lipid specific molecular ion emission as a function of the primary ion characteristics utilizing time-of-flight, secondary ion mass spectrometry (TOF-SIMS). In particular, we revisit the molecular ion emission characteristics for two pairs of small polyatomic and nanoparticle primary ion beams (e.g., Bi_3^+ versus Ar_{1000}^+ and Au_3^+ versus Au_{400}^{+4}) using the secondary ion yield of fragment and intact molecular ions for familiar lipids. Emphasis is made on the relative distribution of lipid-specific fragment ions and molecular ions as a function of the projectile size and energy as well as the matrix effects on the ionization efficiency and secondary ion yields.

II. EXPERIMENT

A. Sample preparation

Lipid standards of sulfatides [131305, Brain, Porcine, (major component 18:1/24:1 ST)], sphingomyelin [860061, Egg, Chicken (major component 18:1/16:0 SM)], 1,2-dipalmitoyl-sn-glycero-3-phosphocholine [850355, (16:0 PC DPPC)], 1-stearoyl-2-oleoyl-sn-glycero-3-phospho-(1′-rac-glycerol) (sodium salt) [840503, (18:0–18:1 PG)], and 1,2-dimyristoyl-sn-glycero-3-phosphoethanolamine [850745, (14:0 PE)] were purchased from Avanti Lipids, Inc. (Alabaster, AL) and used as received. Each standard was dissolved in a dichloromethane: methanol (60:40) solution for a final concentration of 1 mg/mL each. Each standard was deposited onto an ITO slide (Sigma Aldrich, St. Louis, MO) by aerosol spray of 1 ml to guarantee surface homogeneity. The aerosol sprayer was washed with the same solvent solution in between spraying of individual standards. The samples were allowed to dry in a chemical hood prior to SIMS analysis. The same procedure was followed for the preparation of a mixture of lipid standards consisting of sulfatides, SM, DPPC, PE, and PG all equivolume with concentrations of 0.167 mg/ml.

B. SIMS analysis

Standards were analyzed using Bi_3^+, Ar_{1000}^+, Au_3^+, and Au_{400}^{+4} primary ions in positive and negative ionization modes. A commercial IonTOF (Ref. 5) instrument (Chestnut Ridge, NY) containing a hybrid detector with a single microchannel plate, scintillator, and photomultiplier was used for the 25 keV Bi_3^+ and 20 keV $Ar_{500-2000}^+$ analyses. The 25 keV Bi_3^+ (0.12 pA) and 20 keV Ar_{1000}^+ (0.04 pA) primary ion beams were rastered in sawtooth mode over a 250 $\times$ 250 μm^2 field of view, and mass spectra were collected for a total dose density of 2×10^{11} ions/cm^2. Measurements were obtained in the pulsed mode static SIMS at a frequency of 7.7 kHz. The opening time of the second plate of the dual blanking plate has been reduced to obtain a lower beam current for Bi_3^+ and subsequently avoid saturation of the detector. Secondary ion yields were normalized to the number of primary ions used to generate the mass spectral peak or total ion dose. A low energy flood gun is also utilized between pulses to ensure the sample surface remains neutral throughout the analysis. An internal calibration was performed using low mass ions and lipid head groups typically present in the sample: $C_2H_3^+$, $C_2H_5^+$, $C_3H_7^+$, $C_5H_{12}N^+$, and $C_5H_{14}NO^+$ in the positive mode and CH^-, CH_{2-}, OH^-, CN^- Cl^-, CNO^-, PO_2^-, PO_3^-, H_2PO_4, $C_4H_{10}PO_4^-$ in the negative ion mode. For comparison of primary ion beam (Sec. III B), SI yield as a function of primary ion energy (Sec. III C), and SI yield as a function of chemical environment (Sec. III D), triplicate analyses were performed; error bars are calculated by the standard deviation between the SI yields of each replicate. The mass resolution of each primary ion beam was on average 1500 for Ar_{1000}^+ and 4500 for Bi_3^+ at m/z 400. For Au_3^+ and Au_{400}^{+4} analyses, the primary ions were obtained from a 120 kV Pegase Platform,[30–32] equipped with a gold liquid metal ion source capable of producing a variety of projectiles (e.g., 150 nA for Au_1^+, 15 nA for Au_3^+, and 1 nA for Au_{400}^{+4} without beam collimation/pulsing at the target).[33] The primary ion projectiles were mass-selected using a Wien filter and focused into the TOF-SIMS analysis chamber. The negative mode TOF-SIMS was performed in the analysis chamber 1, where the target voltage is held at −10 kV (total acceleration voltage of up to 130 kV), whereas the positive mode TOF-SIMS was performed in analysis chamber 2, where the target voltage is held at +10 kV (total acceleration voltage of up to 110 kV).[33] Further information about the instrumental setup can be found in Refs. 30–33. The average mass resolution for Au_3^+ and Au_{400}^{+4} analyses at m/z 400 is 2000 and 450 in chamber 1 (equipped with a reflectron TOF) and in chamber 2 (equipped with a linear TOF), respectively.

III. RESULTS AND DISCUSSION

A. Lipid characterization by class

TOF-SIMS analysis can provide sufficient information to identify a lipid of a specific class based on the simultaneous detection of analyte specific fragment and intact molecular and/or pseudomolecular ions (e.g., $[M]^+$, $[M+H]^+$,

$[M+Na]^+$, $[M]^-$, and $[M-H]^-$). For example, phospholipids are a class of lipids that are predominantly abundant in biological membranes and consist of two fatty acids, glycerol, phosphate, and an alcohol group. There are several subclasses of phospholipids which differ based on the alcohol moiety present in the molecule (i.e., serine, ethanolamine, choline, glycerol, or inositol). In previous reports, various lipid species, including intact lipids, head group fragments, and fatty acyls, have been identified in cell lines using several mass spectrometry techniques (e.g., ESI-MS/MS, DESI-MS/MS, MALDI-MS/MS, and SIMS). DESI-MS/MS, MALDI-MS/MS, and SIMS have the advantage over traditional ESI-MS/MS in that lipid identification may not require sample extraction protocols and direct analysis can be performed from the biological tissue of interest; while there are major differences between the ionization mechanism of DESI-MS/MS, MALDI-MS/MS, and SIMS, all three techniques can provide spatial information with SIMS providing the highest spatial resolution. A tradeoff is that in the case of TOF-SIMS, the ratio of molecular to fragment ion and the spatial resolution significantly depends on the projectile size and energy as well as on the lipid species of interest and TOF-SIMS analysis mode (positive versus negative). For example, in the positive mode TOF-SIMS, head group fragments corresponding to the sphingomyelin and phosphatidylcholine are identified at *m/z:* 206 $C_5H_{14}NPO_4Na^+$, 184 $C_5H_{15}NPO_4^+$, 104 $C_5H_{14}NO^+$, and 86 $C_5H_{12}N^+$ via TOF-SIMS, ESI-MS/MS [Figs. 1(a) and 1(b)].[1,4,34–41] Both of these lipid classes yield an internal fragment at *m/z* 125 in the positive ionization mode arising from fragmentation of the head group to yield a cyclic $C_2H_6PO_4^+$ fragment.[40,42] The negative mode TOF-SIMS of sphingomyelin and phosphatidylcholine reveals two head group fragments at *m/z* 123 $C_2H_4PO_4^-$ and *m/z* 168 $C_4H_{11}NPO_4^-$.[43] Three larger fragments of higher mass are detected in sphingomyelin analysis related to the loss of methyl $[M\text{-}CH_3]^-$, trimethylamine $[M\text{-}C_3H_9N]^-$, and ethyltrimethylammonium $[M\text{-}C_5H_{13}N]^-$ groups from the head group of the lipid [Figs. 1(a) and S1].[4,42,62] In addition, fragment ions corresponding to the carboxylic acid chain are typically detected from phosphatidylcholine only [see example in Fig. 1(b)]. Lipids in the sphingomyelin and phosphatidylcholine classes have the same head group and therefore cannot be differentiated from each other exclusively based on the head group fragment detection. There are few differences between the ionization of sphingomyelin and phosphatidylcholine by TOF-SIMS; the major difference is attributed to the head group fragment at *m/z* 224 which is not observed in sphingomyelin.[44–47] A second difference in the TOF-SIMS of PC *versus* SM is the presence of fatty acid fragments in the phosphatidylcholine lipid profile in the negative mode, which are not observed in sphingomyelin [Figs. 1(a), 1(b), and 2(f)].

In addition to phosphatidylcholine and sphingomyelin, phosphatidylethanolamine and phosphatidylglycerol fragmentation patterns by TOF-SIMS analysis are described herein. Fragments observed in the phosphatidylethanolamine lipid class include the internal fragments of *m/z* 125 $C_2H_6PO_4^+$ and *m/z* 123 $C_2H_4PO_4^-$ in positive and negative modes, respectively.[40] A tail group fragment after the loss of the head group $[M\text{-}C_2H_7NPO_4]^-$ and the loss of a fatty acid chain $[M\text{-FA Chain}]^-$ were detected [Figs. 1(c) and 2(b)]. Two major characteristic fragments of phosphatidylethanolamine were detected at *m/z* 141 $C_2H_8NPO_4^+$,[43] and *m/z* 140 $C_2H_7NPO_4^-$ and *m/z* 196 $C_5H_{11}NPO_5^-$ (Ref. 43) in positive and negative TOF-SIMS modes, respectively, allowing for identification of the phosphatidylethanolamine class versus all other lipids considered in this study.

Analysis of phosphatidylglycerol in the positive mode TOF-SIMS yields the cyclic head group fragment at *m/z* 125 $C_2H_6PO_4^+$ as well as the sodiated form of that fragment ion at *m/z* 147 $C_2H_6PO_4Na^+$.[48] Fragments at *m/z* 171 $C_6H_8PO_6^-$ and *m/z* 152 $C_3H_6PO_5^-$ are characteristic fragments significant to the phosphatidylglycerol class in the negative mode TOF-SIMS. A *m/z* 227 $C_6H_{12}PO_7^-$ is also observed corresponding to the loss of both fatty acid chains from the phosphatidylglycerol lipid in the negative mode TOF-SIMS [Figs. 1(d) and 2(c)].[49] The sulfatide class is typically analyzed in the negative mode TOF-SIMS. Characteristic fragments are detected for the head group at *m/z*: 97 HSO_4^-, 199 $C_4H_7O_7S^-$, 225 $C_6H_9O_7S^-$, 257 $C_6H_9O_9S^-$, 259 $C_6H_{11}O_9S^-$, and 300 $C_8H_{14}NO_9^-$. All head group fragments are specific to the sulfatides due to the presence of a sulfur atom. A mixture of sulfatides with varying fatty acid composition results in the observation of a variety of intact molecular ions [Figs. 2(e) and S2].[62]

Fatty acid chains are typically observed in the negative mode TOF-SIMS in phosphatidylethanolamine, phosphatidylglycerol, phosphatidylcholine, and sulfatides. For example, phosphatidylethanolamine and phosphatidylglycerol analyses show peaks at *m/z* 227 $C_{14}H_{29}O_2^-$ and *m/z* 283 $C_{18}H_{35}O^-$ corresponding to the 14:0 and 18:0 fatty acid chain fragments [Figs. 1(c) and 2(a)]. The sulfatide standard contains a mixture of lipids and fatty acid fragments, and peaks are observed in the mixture at *m/z* 255 (16:0), *m/z* 283 (18:0) and *m/z* 311 (20:0) [Figs. 2(e) and S2].[62] By combining the information obtained from the head group fragments, fragment fatty acid chains, tail group fragment, loss of a fatty acid chain, and the pseudomolecular ions, it may be possible to directly correlate the TOF-SIMS spectral features to the lipid structure in complex biological matrices. The latter analysis can be simplified further when using coincidence TOF-SIMS techniques during single ion bombardment.[50]

B. SI yield as a function of the projectile size

Lipid standards were analyzed as a function of the projectile size (Bi_3^+ and Au_3^+, Ar_{1000}^+, and Au_{400}^{+4}) and energy. An increase in secondary ion yield (SI yield) was observed between small polyatomic and nanoparticle projectiles throughout all lipid classes in positive and negative ionization modes (see, for example, Bi_3^+ and Ar_{1000}^+ in Fig. 3). In the sulfatide class, over tenfold increase is observed for 20 keV Ar_{1000}^+ when compared to 25 keV Bi_3^+ in the negative mode TOF-SIMS. The $[M-H]^-$ SI yields of the other lipids showed an increase when going from Bi_3^+ to Ar_{1000}^+ primary ions, but most of the changes were not as large as

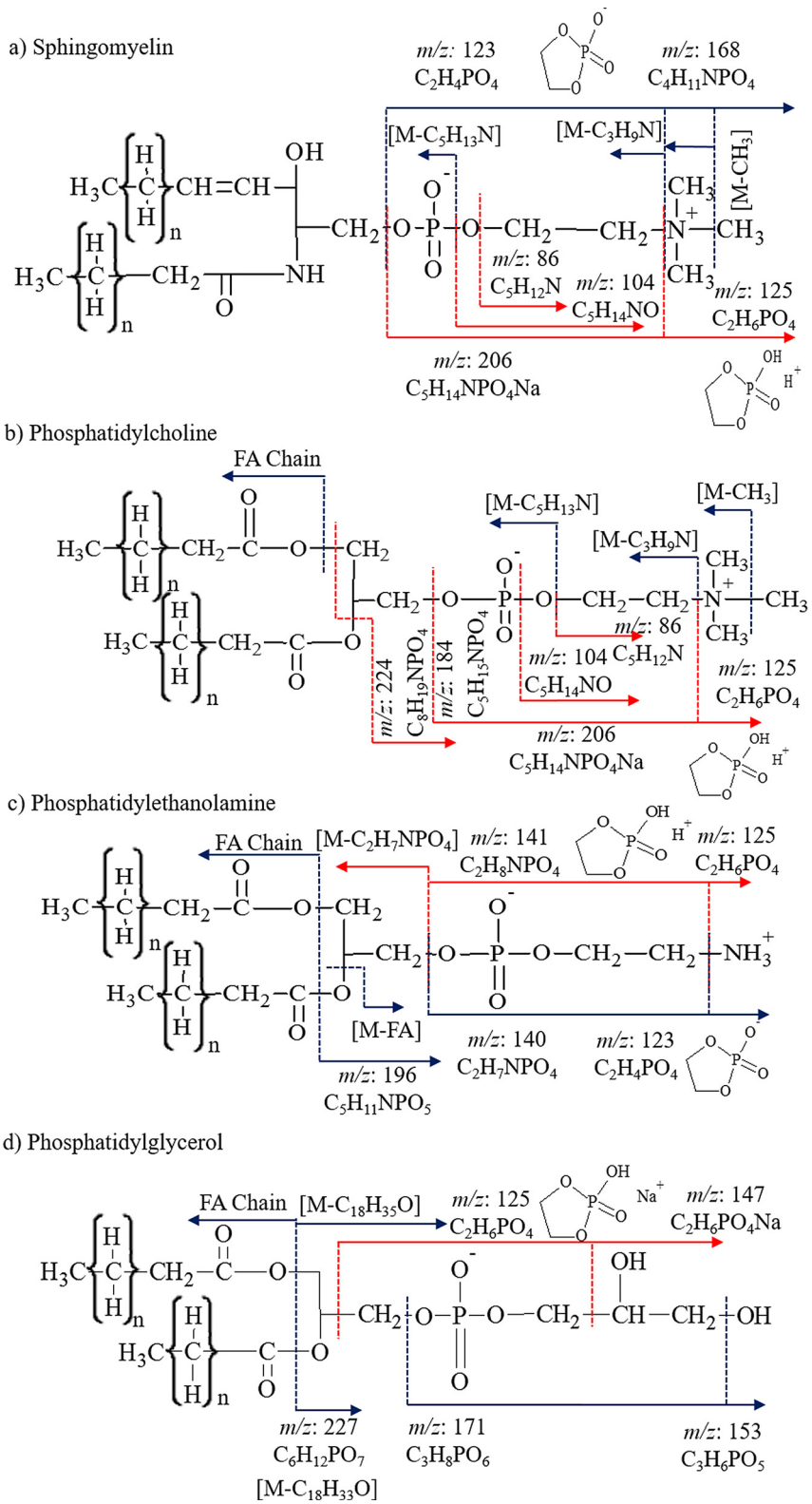

FIG. 1. (Color online) Fragmentation schemes of lipid standards of (a) sphingomyelin, (b) phosphatidylcholine, (c) phosphatidylethanolamine, and (d) phosphatidylglycerol for positive (red) and negative (blue) mode TOF-SIMS analyses.

those seen in the ST class [Fig. 3(a)]. In the cases of sphingomyelin and phosphatidylethanolamine, the SI yield of the $[M\text{-}H]^-$ molecular ion had less than an order of magnitude of change in abundance, whereas phosphatidylglycerol and phosphatidylcholine had a more significant abundance increase. Phosphatidylcholine had the second largest increase in SI yield when changing from Bi_3^+ to Ar_{1000}^+ primary ions. SI signal enhancements were previously reported for argon clusters relative to bismuth clusters for the analysis of biological molecules (diadenosine triphosphate and

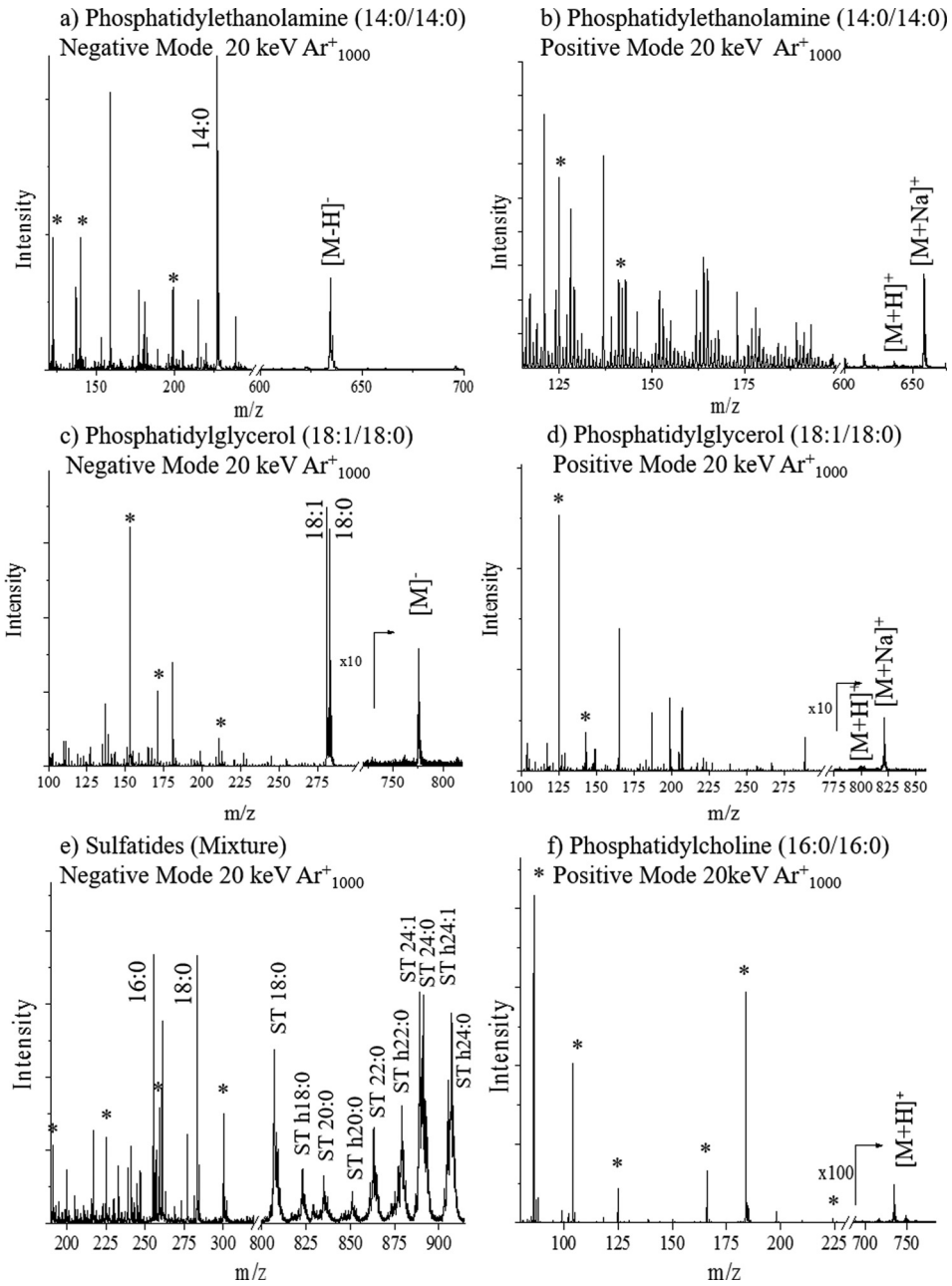

FIG. 2. Typical TOF-SIMS mass spectra of familiar lipids in positive and negative modes. Characteristic fragment ions (*), fatty acid fragments, and intact molecular ions are denoted in the spectra.

diadenosine tetraphosphate).[51] In the positive mode TOF-SIMS, a different trend is observed for SI yield variation with the primary ion projectile size [see Fig. 3(b)]. The only protonated molecular ion showing significant differences in the SI yield corresponds to the sphingomyelin class. The remaining $[M+H]^+$ molecular ions of the lipids do not show significant changes in SI yield using the two different primary ion beams. A variation between the SI yields of the intact lipid molecular ion ($[M-H]^-/[M+H]^+$) of each lipid class is observed for both positive and negative mode TOF-SIMS; however, the negative mode TOF-SIMS shows greater variation in the SI yields (Fig. 3). The increase in SI yield with the Ar_{1000}^+ beam can be attributed to the softer desorption regime compared to that of Bi_3^+. The E_{atom} for each beam is discussed in detail later; however, in the examples shown, the Ar_{1000}^+ beam has an energy per atom closest to that deemed the ideal ($E_{atom} = 10$ eV/atom).[15]

The comparison of SI yields of lipids using gold projectiles showed that the nanoparticle projectile Au_{400}^{+4} may provide over tenfold increase in the SI yield when compared to the small polyatomic projectile Au_3^+ (Table S1).[62] For example, during sulfatide analysis, the intact molecular ion (ST 40:1) showed a 100-fold increase in the secondary ion yield from 50 keV Au_3^+ to 440 keV Au_{400}^{+4} and a tenfold increase for the smaller gold beam when compared to 25 keV Bi_3^+ (Table S1).[62] There is a 2–3 order of magnitude increase in the SI yield when using 440 keV Au_{400}^{+4} versus 20 keV Ar_{1000}^+ that can be primarily attributed to the

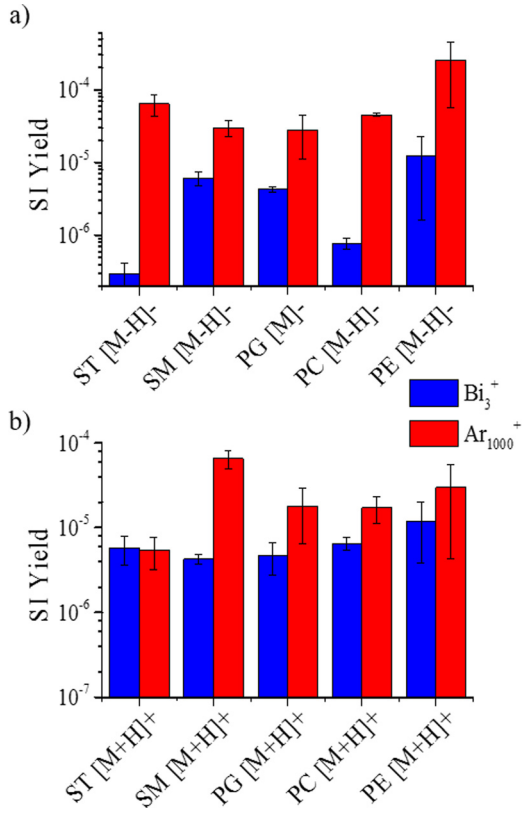

FIG. 3. (Color online) Intact molecular ion SI yield emission using small polyatomic Bi_3^+ and nanoparticle Ar_{1000}^+ primary ion projectiles for familiar lipid standards using TOF-SIMS in (a) negative and (b) positive modes.

incident energy of the projectile (Table S1).[62] Overall, the analysis of lipids using Au_{400}^{+4} followed the same trend with a 2 order of magnitude increase in SI yield compared to Au_3^+ (Tables S1 and S2).[62] SI yields of 440 keV Au_{400}^{+4} were 2–3 orders of magnitude higher than those obtained using the Ar_{1000}^+ primary ion beam for most lipid classes (e.g., sphingomyelin, phosphatidylglycerol, phosphatidylcholine, and phosphatidylethanolamine, see Table S1).[62] It has been previously noted that the estimated Au_3^+ SI yields would be equal to Bi_3^+ yields because they are of similar nature and size.[52] For a more detailed analysis, the E_{atom} needs to be considered due to the large differences in energies used for each primary ion beam. For the small polyatomic projectiles, the E_{atom} are calculated at approximately 8000 and 16 000 eV for Bi_3^+ and Au_3^+, respectively. Our results suggest that the larger the E_{atom} for small polyatomic projectiles, the larger the SI yield. A discussion of the SI yield as a function of the energy and cluster size is provided for the $Ar_{n=500-2000}^+$ and Au_{400}^{+4} nanoparticle projectiles.

C. SI yield as a function of the projectile energy

Previous work has shown that high energy, massive gold projectiles are advantageous for biological sample analysis and that the higher the cluster size the higher the SI yield.[32] This correlates to data obtained by Vickerman *et al.* and by Yokoyama *et al.* where SI yields of both metals and organic substances increases with the primary ion impact energy (up to 120 keV for C_{60} projectiles), being most notable for higher mass fragments.[53,54] Here, we further investigate the effect of the primary ion energy and size on the SI yield for the case of the phosphatidylglycerol (18:0–18:1 PG) lipid standard (see Fig. 4). Two studies are carried out: (1) the influence of the projectile energy on the SI yield for nanoparticle Au_{400}^{+4} projectiles, and (2) the influence of the projectile size on the SI yield for 20 keV Ar_n^+ (n = 500–2000 atoms) projectiles.

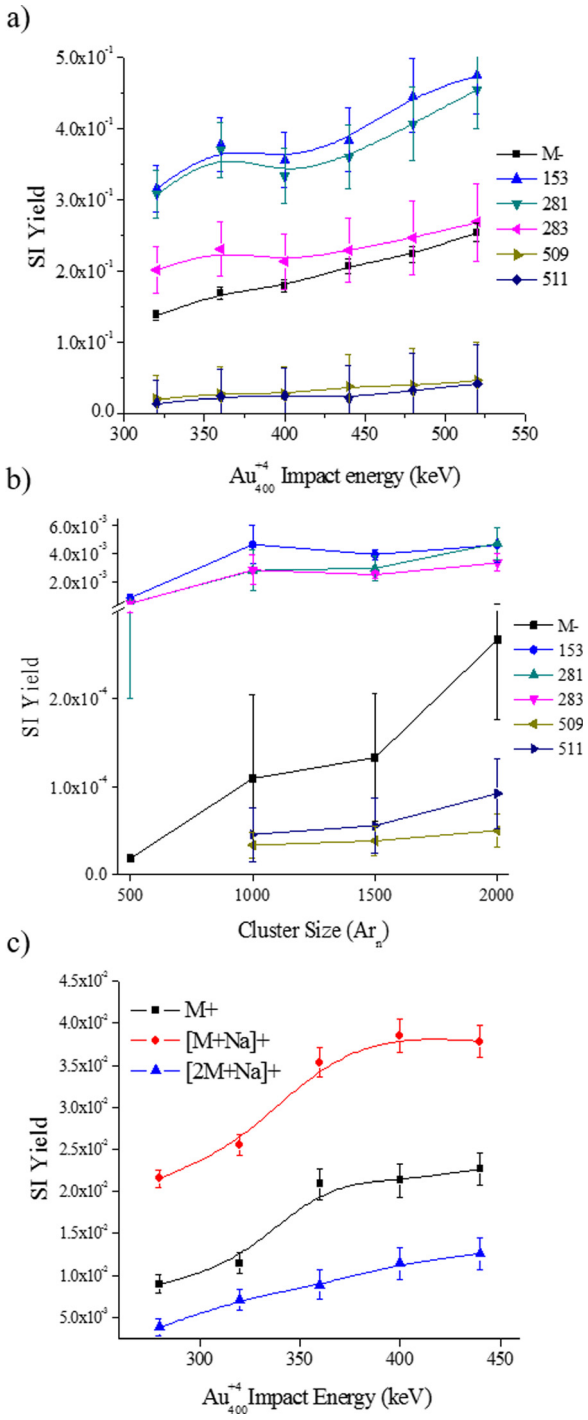

FIG. 4. (Color online) Secondary ion yields as a function of the nanoparticle Au_{400}^{+4} projectile energy or Ar_n^+ cluster size for a lipid model target of phosphatidylglycerol (18:0–18:1 PG) (a) Au_{400}^+ and (b) Ar_n^+ negative and (c) Au_{400}^+ positive mode. Notice the break in vertical axis in (b).

In positive and negative mode TOF-SIMS, as the primary Au_{400}^{4+} ion energy increases, there is a net SI yield increase of molecular and fragment ions [Figs. 4(a) and 4(c)]. For example, in the negative mode TOF-SIMS, closer inspection shows that small (*m*/*z*: 153, 281, and 283) and larger (*m*/*z* 509 and 511) mass fragments show a slightly different increasing slope, being a steeper positive slope for the smaller fragments [see Fig. S3(a) and Table S3].[62] Notice that analyte-specific fragment ions corresponds to the head group (*m*/*z* 153), fatty acid groups (*m*/*z* 281 and 283 for 18:1 and 18:0, respectively), and the loss of one fatty acid group (*m*/*z* 509 and 511). For the low mass fragments, results show that as the Au_{400}^{4+} ion energy increases the ratio of molecular to fragment ion increases in a nonlinear fashion. That is, the SI yield of $[M]^-$ increases more than the SI yield of the low mass fragments. For the higher mass fragments (*m*/*z* 509 and 511), the opposite trend is observed where the ratio of $[M]^-$ to larger fragment ions decreases. We interpret the difference in slopes between the low (*m*/*z* 153, 281 and 283) and higher (*m*/*z* 509 and 511) mass fragments as a decrease of the internal energy distribution of the molecular ions with the projectile energy increase due to a larger emission volume (the larger the volume the lower the energy per emitted species). That is, as the projectile energy increases, the larger desorption volume leads to a lower internal energy distribution which favors the production of higher mass fragments and intact molecular ions. In the positive mode TOF-SIMS, the molecular ion emission also increases with the Au_{400}^{+4} projectile energies. Closer inspection shows that as the Au_{400}^{4+} ion energy increases a proportional increase in M^+, $[M+Na]^+$, and $[2M+Na]^+$ emission is observed [Fig. 4(c) and Table S5].[62] These positive and negative mode TOF-SIMS results suggest that as the Au_{400}^{+4} E_{atom} increases the nanoparticle penetration into the sample increases, thus creating a larger emission volume in a way that scales the emission of intact molecular and higher mass fragment ions as a consequence of the lower internal energy of the emitted species.

In a different scenario, an increase of the 20 keV Ar_n^+ cluster size from 500 to 2000 atoms (or decrease in the E_{atom}) results in an increase in SI yield of M^-, head group fragments, and fatty acid fragments [Fig. 4(b)]. The SI yield of the molecular ion is rising at a faster rate than all of the fragment ions as the cluster size ranges from 500 to 2000 argon atoms, being the most significant between Ar_{1500} and Ar_{2000} [Fig. 4(b), Tables S4 and S3b]. This SI yield dependence on the Ar_n^+ cluster size is in good agreement with recent observations by Yokoyama *et al.* using 20 keV $Ar_{n=2000-5000}$ cluster impacts.[54] Previous report of Ar_n cluster impacts at 10–40 eV/atom has also shown that larger fragments are more favorable with the increase in Ar_n projectile size.[18] These results suggest that as the size of the Ar_n^+ projectile increases a larger impact cross section is achieved that enhances the emission volume; the weak forces that hold the Ar_n cluster together do not lead to penetration/implantation into the surface. Notice that this mechanism is very different from that of the nanoparticle Au_{400}^{+4} projectiles.

D. SI yield as a function of chemical environment

SIMS is a very useful mass spectrometry tool for the analysis of biological matrices as previously described.[2,16,18,32,43,55,56] The chemical environment (matrix) of compounds of interest has a significant impact on the limit of detection, ionization efficiency, and ion suppression for TOF-SIMS and for other ionization sources.[57] To evaluate the influence a matrix has on the SI yield, we compared the emission from the single lipid component sample to the emission from a sample containing a mixture of all five-lipid classes at equal concentrations. The protonated and deprotonated molecular ion of each lipid was utilized for comparison in positive and negative mode TOF-SIMS, respectively. The analysis of the sulfatides mixture in negative and positive mode TOF-SIMS using Ar_{1000}^+ showed no suppression or enhancement for the deprotonated/protonated molecular ion [Figs. 5(a) and 5(b)]. For Bi_3^+ analysis, in the negative mode TOF-SIMS, ion enhancement is observed for the sulfatides and in the positive TOF-SIMS no change is observed from the single standard to the mixture [Figs. 5(d) and 5(c)]. Typically, sulfatides are preferentially ionized in negative ionization mode and this could contribute to the fact that opposite trends are observed between the two ionization modes for Bi_3 analysis. For a characteristic ion of the sulfatide lipid class (HSO_4^-), the SI yields of the fragments are on the same order of magnitude in both, alone and as a mixture using Ar_{1000}^+ and Bi_3^+projectiles (data not shown). For the sphingomyelin class of lipids, the positive mode TOF-SIMS shows no suppression in the SI yield of the $[M+H]^+$; however, in the negative mode TOF-SIMS, an order of magnitude decrease is observed between the SI yield of the single lipid and the SI yield of the lipid mixture [Figs. 5(a) and 5(b)]. Using the Bi_3^+ projectiles, no significant changes are observed between single lipid and lipid mixture analysis of sphingomyelin in the positive ionization mode TOF-SIMS and a slight decrease in SI yield is observed in the negative mode TOF-SIMS [Figs. 5(c) and 5(d)].

The analysis of phosphatidylglycerol in the positive mode TOF-SIMS demonstrates no significant changes with the Ar_{1000}^+ projectiles and a small decrease in SI yield using the Bi_3^+ projectiles [Figs. 5(a) and 5(c)]. For the analysis of phosphatidylglycerol in the negative mode TOF-SIMS, no ionization suppression or enhancement is observed for either of the primary ion projectiles [Figs. 5(b) and 5(d)]. SI yields of characteristic fragment peaks for phosphatidylglycerol (i.e., *m*/*z* 153 and 171) also showed no change between single and mixture conditions (data not shown). As previously mentioned, phosphatidylcholine is a lipid typically analyzed in the positive mode TOF-SIMS; in the positive mode TOF-SIMS, the SI yield of the $[M+H]^+$ ion does not show a major matrix effect and no large changes in ion abundance are observed for Ar_{1000}^+ or Bi_3^+ [Figs. 5(a) and 5(c)]. In the negative mode TOF-SIMS, a different trend is seen for phosphatidylcholine, with suppression in the mixture signal observed using Ar_{1000}^+ and an enhancement in SI yield observed for Bi_3^+ projectiles [Figs. 5(b) and 5(d)]; this difference in trend between the positive and negative mode TOF-SIMS could be attributed to the fact that

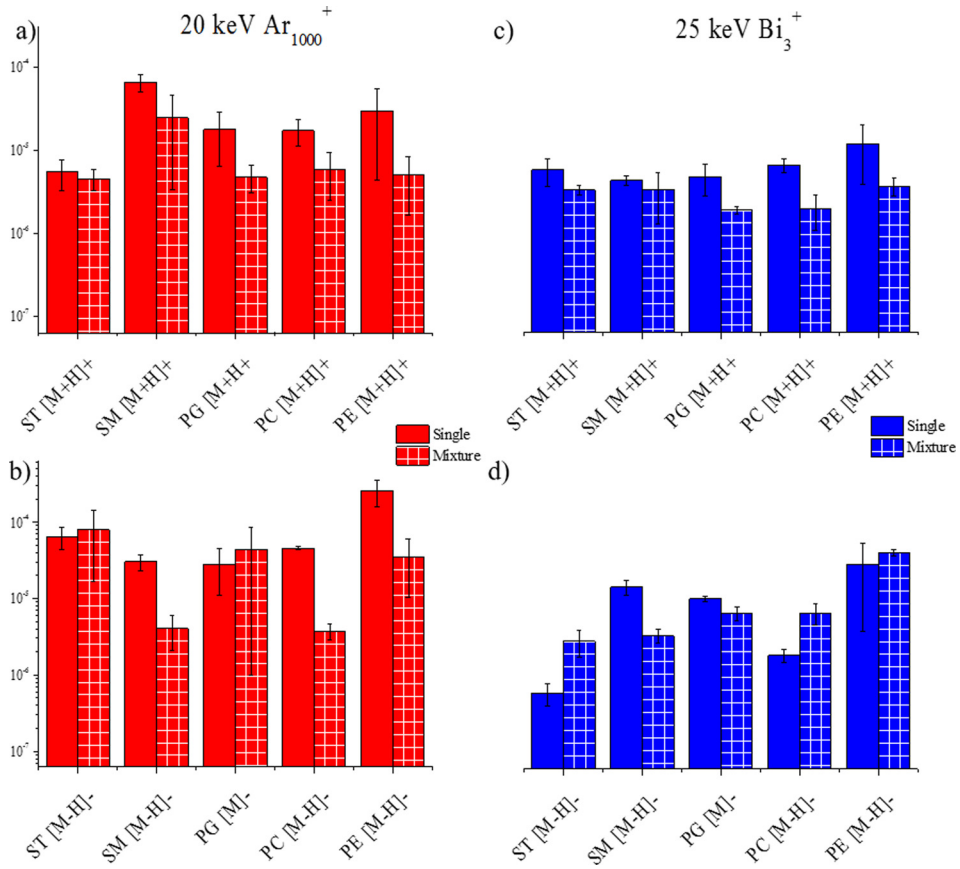

FIG. 5. (Color online) Secondary ion yields of intact molecular ions from a single lipid standard sample and a mixture of lipid standards sample in (a) positive mode Ar_{1000}^{+}, (b) negative mode Ar_{1000}^{+}, (c) positive mode Bi_3^{+}, and (d) negative mode Bi_3^{+}.

phosphatidylcholine is preferentially ionized in the positive mode TOF-SIMS. A previous study by Jones *et al*. of matrix effects in TOF-SIMS used phosphatidylcholine as a complex matrix while looking for targeted drug analytes.[57] It was determined that the lipid had a very strong suppression effect on the abundance of the molecular ion of the drug due to its proton affinity.[57] In our study, we observed a similar suppression effect on the pseudomolecular ions of the lipids in the mixture, potentially from the presence of phosphatidylcholine [Figs. 5(a) and 5(b)]. For the analysis of phosphatidylethanolamine by Ar_{1000}^{+}, there is less than tenfold suppression of ion signal going from the single lipid to the mixture of lipids [Figs. 5(a) and 5(b)]. No major changes are observed using Bi_3^{+} for the $[M-H]^{-}$ or $[M+H]^{+}$ from phosphatidylethanolamine [Figs. 5(c) and 5(d)]. No major changes in SI yield are seen for the characteristic peaks (*m*/*z* 141 and 196) of the phosphatidylethanolamine lipid class. In general, these matrix studies have shown that matrix effects are minimal on the SI yield of lipid standards when the lipid is analyzed in either ionization polarity. According to previous studies, chemical environment of a sample has a large impact on the SI yield of targeted molecules as shown with the large suppressive effects phosphatidylcholine has on the M and the enhancement effects cholesterol induced when used as a comparative matrix.[57,58] More recently, matrix enhanced TOF-SIMS has been developed in order to more easily and efficiently ionize samples within complex biological matrices via TOF-SIMS.[57,59–61] Our studies suggest that the secondary ion yield of the molecular ion of lipids from a single standard or from a mixture of lipids does not significantly change with the primary ion identity in the positive ion mode TOF-SIMS and slightly decreases in the negative ion mode TOF-SIMS.

IV. SUMMARY AND CONCLUSIONS

In this paper, we provide detailed information on the TOF-SIMS fragmentation pattern for sphingomyelins, phosphatidylcholine, phosphatidylglycerol, sulfatides, and phosphatidylethanolamine lipid classes. Typical mass spectra for common lipids are shown and discussed based on their fragmentation patterns. Changes in secondary ion yields were analyzed as a function of the primary ion (Bi_3^{+} versus Ar_{1000}^{+} and Au_3^{+} versus Au_{400}^{+4}) using TOF-SIMS. For the case of lipid analysis, the results suggest that for polyatomic projectiles (Bi_3^{+} and Au_3^{+}), the increase in the primary ion energy leads to an increase in the SI yield. However, larger SI yields are obtained for molecular ions using nanoparticle projectiles. Two different trends were observed in the case of the nanoparticle projectiles (Ar_n^{+} and Au_{400}^{+4}) that may be related to their intramolecular forces. For example, in the case of Au_{400}^{+4} projectiles, as the projectile energy increases, a larger SI yield is observed for fragment and molecular ions, with small variation on their relative ratio. That is, the larger the E_{atom} for Au_{400}^{+4} projectiles the larger

the SI yield. In the case of the Ar_n^+ projectiles, the lower the E_{atom} the larger the SI yield. We interpret these effects as consequence of two ways to increase the desorption volume: (1) larger incident energy for Au_{400}^{+4} projectiles leads to a larger penetration depth and emission volume, and (2) a larger Ar_n^+ cluster size (larger number of atoms) yields a larger impact cross section and emission volume. Overall, the matrix studies showed that the sample composition has a minimal effect on the desorption yields of intact molecular ions of familiar lipids and primary ion identity shows no significant effects of the secondary ion yield in the positive ion mode TOF-SIMS and a slight decrease in the negative ion mode TOF-SIMS. This work further provides more information on the main factors that affect the SI yield as well as characteristic patterns that allow lipid analysis in biological environments using TOF-SIMS.

ACKNOWLEDGMENTS

This work was supported by NIGMS grant GM106414 to FF-L. The authors acknowledge the support of Emile Schweikert and Serge Della-Negra during the acquisition of the Au_3^+/Au_{400}^{+4} data in the 120 kV Pegasus platform at Texas A&M University and for helpful discussions.

[1]M. K. Passarelli and N. Winograd, Biochim. Biophys. Acta **1811**, 976 (2011).
[2]J. D. DeBord, D. F. Smith, C. R. Anderton, R. M. Heeren, L. Pasa-Tolic, R. H. Gomer, and F. A. Fernandez-Lima, PLoS One **9**, e99319 (2014).
[3]H.-Y. Nie, J. Francis, A. Taylor, M. Walzak, W. Chang, D. MacFabe, and W. Lau, Appl. Surf. Sci. **255**, 1079 (2008).
[4]M. Saleem and H.-J. Galla, Biochim. Biophys. Acta **1798**, 730 (2010).
[5]D. Touboul, A. Brunelle, F. Halgand, S. De La Porte, and O. Laprévote, J. Lipid Res. **46**, 1388 (2005).
[6]D. Touboul, F. Halgand, A. Brunelle, R. Kersting, E. Tallarek, B. Hagenhoff, and O. Laprévote, Anal. Chem. **76**, 1550 (2004).
[7]S. Rabbani, A. M. Barber, J. S. Fletcher, N. P. Lockyer, and J. C. Vickerman, Anal. Chem. **83**, 3793 (2011).
[8]S. Ninomiya, K. Ichiki, H. Yamada, Y. Nakata, T. Seki, T. Aoki, and J. Matsuo, Rapid Commun. Mass Spectrom. **23**, 1601 (2009).
[9]I. Yamada, J. Matsuo, N. Toyoda, and A. Kirkpatrick, Mater. Sci. Eng., R **34**, 231 (2001).
[10]C. Lechene *et al.*, J. Biol. **5**, 20.1 (2006).
[11]R. M. Braun, A. Beyder, J. Xu, M. C. Wood, A. G. Ewing, and N. Winograd, Anal. Chem. **71**, 3318 (1999).
[12]S. G. Boxer, M. L. Kraft, and P. K. Weber, Annu. Rev. Biophys. **38**, 53 (2009).
[13]E. Schweikert, M. J. van Stipdonk, and R. D. Harris, Rapid Commun. Mass Spectrom. **10**, 1987 (1996).
[14]S. Sheraz née Rabbani, A. Barber, J. S. Fletcher, N. P. Lockyer, and J. C. Vickerman, Anal. Chem. **85**, 5654 (2013).
[15]S. Sheraz née Rabbani, I. B. Razo, T. Kohn, N. P. Lockyer, and J. C. Vickerman, Anal. Chem. **87**, 2367 (2015).
[16]J. S. Fletcher, N. P. Lockyer, and J. C. Vickerman, Mass Spectrom. Rev. **30**, 142 (2011).
[17]D. Gode and D. A. Volmer, Analyst **138**, 1289 (2013).
[18]S. Aoyagi, J. S. Fletcher, S. Sheraz, T. Kawashima, I. B. Razo, A. Henderson, N. P. Lockyer, and J. C. Vickerman, Anal. Bioanal. Chem. **405**, 6621 (2013).
[19]C. Wolf and P. J. Quinn, Prog. Lipid Res. **47**, 15 (2008).
[20]M. R. Wenk, Cell **143**, 888 (2010).
[21]E. Layre and D. B. Moody, Biochimie **95**, 109 (2013).
[22]E. R. Schenk, F. Nau, C. J. Thompson, Y.-C. Tse-Dinh, and F. Fernandez-Lima, J. Mass Spectrom. **50**, 88 (2015).
[23]E. Fahy *et al.*, J. Lipid Res. **46**, 839 (2005).
[24]E. Fahy *et al.*, J. Lipid Res. **50**, S9 (2009).
[25]K. Schmelzer, E. Fahy, S. Subramaniam, and E. A. Dennis, Methods Enzymol. **432**, 171 (2007).
[26]A. Wucher, Appl. Surf. Sci. **252**, 6482 (2006).
[27]N. Wehbe, M. Fallavier, S. Della-Negra, J. Depauw, A. Brunelle, and H. H. Andersen, Nucl. Instrum. Methods Phys. Res., Sect. B **268**, 2596 (2010).
[28]M. L. Pacholski, D. M. Cannon, A. G. Ewing, and N. Winograd, Rapid Commun. Mass Spectrom. **12**, 1232 (1998).
[29]T. B. Angerer, P. Blenkinsopp, and J. S. Fletcher, Int. J. Mass Spectrom. **377**, 591 (2015).
[30]S. Della-Negra, J. Arianer, J. Depauw, S. Verkhoturov, and E. Schweikert, Surf. Interface Anal. **43**, 66 (2011).
[31]F. Fernandez-Lima, M. Eller, J. DeBord, S. Verkhoturov, S. Della-Negra, and E. Schweikert, Nucl. Instrum. Methods Phys. Res., Sect. B **273**, 270 (2012).
[32]F. A. Fernandez-Lima, J. Post, J. D. DeBord, M. J. Eller, S. V. Verkhoturov, S. Della-Negra, A. S. Woods, and E. A. Schweikert, Anal. Chem. **83**, 8448 (2011).
[33]S. Bouneau, S. Della-Negra, J. Depauw, D. Jacquet, Y. Le Beyec, J. P. Mouffron, A. Novikov, and M. Pautrat, Nucl. Instrum. Methods Phys. Res., Sect. B **225**, 579 (2004).
[34]T. P. Roddy, D. M. Cannon, C. A. Meserole, N. Winograd, and A. G. Ewing, Anal. Chem. **74**, 4011 (2002).
[35]H. J. Yang, Y. Sugiura, I. Ishizaki, N. Sanada, K. Ikegami, N. Zaima, K. Shrivas, and M. Setou, Surf. Interface Anal. **42**, 1606 (2010).
[36]H.-J. Yang, I. Ishizaki, N. Sanada, N. Zaima, Y. Sugiura, I. Yao, K. Ikegami, and M. Setou, Med. Mol. Morphol. **43**, 158 (2010).
[37]J. S. Fletcher, N. P. Lockyer, S. Vaidyanathan, and J. C. Vickerman, Anal. Chem. **79**, 2199 (2007).
[38]P. Sjövall, J. Lausmaa, H. Nygren, L. Carlsson, and P. Malmberg, Anal. Chem. **75**, 3429 (2003).
[39]M. E. Kurczy, J. Kozole, S. Parry, P. Piehowski, N. Winograd, and A. Ewing, Appl. Surf. Sci. **255**, 1158 (2008).
[40]S. G. Ostrowski, C. Szakal, J. Kozole, T. P. Roddy, J. Xu, A. G. Ewing, and N. Winograd, Anal. Chem. **77**, 6190 (2005).
[41]O. A. Ismaiel, M. S. Halquist, M. Y. Elmamly, A. Shalaby, and H. T. Karnes, J. Chromatogr. B **875**, 333 (2008).
[42]P. Domingues, F. M. Amado, M. G. O. Santana-Marques, and A. Ferrer-Correia, J. Am. Soc. Mass Spectrom. **9**, 1189 (1998).
[43]B. Brügger, G. Erben, R. Sandhoff, F. T. Wieland, and W. D. Lehmann, Proc. Natl. Acad. Sci. U. S. A. **94**, 2339 (1997).
[44]L. Zheng, C. M. McQuaw, A. G. Ewing, and N. Winograd, J. Am. Chem. Soc. **129**, 15730 (2007).
[45]T. P. Roddy, D. M. Cannon, S. G. Ostrowski, A. G. Ewing, and N. Winograd, Anal. Chem. **75**, 4087 (2003).
[46]D. Touboul, A. Brunelle, and O. Laprévote, Rapid Commun. Mass Spectrom. **20**, 703 (2006).
[47]N. Tahallah, A. Brunelle, S. De La Porte, and O. Laprévote, J. Lipid Res. **49**, 438 (2008).
[48]F.-F. Hsu and J. Turk, J. Am. Soc. Mass Spectrom. **11**, 437 (2000).
[49]F.-F. Hsu and J. Turk, J. Am. Soc. Mass Spectrom. **12**, 1036 (2001).
[50]M. A. Park, K. A. Gibson, K. Quinones, and M. A. Schweikert, Science **248**, 988 (1990).
[51]H. K. Shon, Y. L. Cho, C. S. Lim, J. S. Choi, S. J. Chung, and T. G. Lee, Surf. Interface Anal. **46**, 189 (2014).
[52]D. Touboul, F. Kollmer, E. Niehuis, A. Brunelle, and O. Laprévote, J. Am. Soc. Mass Spectrom. **16**, 1608 (2005).
[53]J. S. Fletcher, X. A. Conlan, E. A. Jones, G. Biddulph, N. P. Lockyer, and J. C. Vickerman, Anal. Chem. **78**, 1827 (2006).
[54]Y. Yokoyama *et al.*, Anal. Chem. **88**, 3592 (2016).
[55]C. Bich, R. Havelund, R. Moellers, D. Touboul, F. Kollmer, E. Niehuis, I. S. Gilmore, and A. Brunelle, Anal. Chem. **85**, 7745 (2013).
[56]T. M. Annesley, Clin. Chem. **49**, 1041 (2003).
[57]E. Jones, N. Lockyer, and J. Vickerman, Appl. Surf. Sci. **252**, 6727 (2006).
[58]E. A. Jones, J. S. Fletcher, C. E. Thompson, D. A. Jackson, N. P. Lockyer, and J. C. Vickerman, Appl. Surf. Sci. **252**, 6844 (2006).
[59]A. F. M. Altelaar, J. van Minnen, C. R. Jiménez, R. M. A. Heeren, and S. R. Piersma, Anal. Chem. **77**, 735 (2005).
[60]J. Cheng and N. Winograd, Anal. Chem. **77**, 3651 (2005).
[61]J. S. Fletcher, A. Henderson, G. X. Biddulph, S. Vaidyanathan, N. P. Lockyer, and J. C. Vickerman, Appl. Surf. Sci. **255**, 1264 (2008).
[62]See supplementary material at http://dx.doi.org/10.1116/1.4961461 for additional tables and figures referred to in the text.